ATLAS NOTE

ATLAS-CONF-2011-086

June 3, 2011

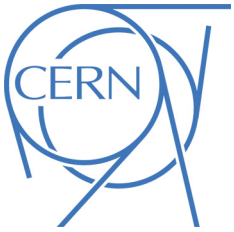

Search for squarks and gluinos using final states with jets and missing transverse momentum with the ATLAS detector in $\sqrt{s}$ = 7 TeV proton-proton collisions

ATLAS Collaboration

Abstract

A search for squarks and gluinos in final states containing jets, missing transverse momentum and no electrons or muons is presented. The data were recorded in 2011 by the ATLAS experiment in $\sqrt{s}$ = 7 TeV proton-proton collisions at the Large Hadron Collider. No excess above the Standard Model background expectation was observed in 165 pb^{-1} of analysed data. Gluino masses below 725 GeV are excluded at the 95% confidence level in simplified models containing only squarks of the first two generations, a gluino octet and a massless neutralino. The exclusion increases to 1025 GeV for equal mass squarks and gluinos. In MSUGRA/CMSSM models with $\tan\beta = 10$, $A_0 = 0$ and $\mu > 0$, squarks and gluinos of equal mass are excluded for masses below 950 GeV. These limits considerably extend the region of supersymmetric parameter space excluded by previous measurements with the ATLAS detector.

1 Introduction

Many extensions of the Standard Model (SM) include heavy coloured particles, some of which could be accessible at the Large Hadron Collider (LHC) [1]. The squarks and gluinos of supersymmetric (SUSY) theories [2] are one class of such particles. This letter presents a new ATLAS search for squarks and gluinos in final states containing only jets and large missing transverse momentum. Interest in this final state is motivated by the large number of R-parity conserving models [3] in which squarks, $\tilde{q}$, and gluinos, $\tilde{g}$, can be produced in pairs $\{\tilde{g}\tilde{g}, \tilde{q}\tilde{q}, \tilde{q}\tilde{g}\}$ and can generate that final state in their decays $\tilde{q} \to q\tilde{\chi}_1^0$ and $\tilde{g} \to qq\tilde{\chi}_1^0$ to weakly interacting neutralinos, $\tilde{\chi}_1^0$, which escape the detector unseen. The analysis presented here is based on a study of purely hadronic final states; events with reconstructed electrons and muons are vetoed to avoid overlap with a related ATLAS search [4] which requires them. This updated analysis uses 165 pb^{-1}of data from 2011 and extends the sensitivity of the search by including final state topologies with at least 4 jets. The statistical analysis benefits from an improved technique which uses a combined likelihood fit across all the signal and control regions to take into account correlations between the measurements. The search strategy was optimised for maximum discovery reach in the $(m_{\tilde{g}}, m_{\tilde{q}})$-plane for a set of simplified models in which all other supersymmetric particles (except for the lightest neutralino) were given masses beyond the reach of the LHC. Although interpreted in terms of supersymmetric models, the main results of this analysis (the data and expected background event counts in the signal regions) are relevant for excluding any model of new physics that predicts production of jets in association with missing transverse momentum. Currently, the most stringent limits on squark and gluino masses are obtained at the LHC [5, 6] and at the Tevatron [7–12].

2 The ATLAS Detector and Data Samples

The ATLAS detector [13] is a multipurpose particle physics apparatus with a forward-backward symmetric cylindrical geometry and nearly 4π coverage in solid angle.[1] The layout of the detector is dominated by four superconducting magnet systems, which comprise a thin solenoid surrounding inner tracking detectors and three large toroids supporting a large muon tracker. The calorimeters are of particular importance to this analysis. In the pseudorapidity region $|\eta| < 3.2$, high-granularity liquid-argon (LAr) electromagnetic (EM) sampling calorimeters are used. An iron-scintillator tile calorimeter provides hadronic coverage over $|\eta| < 1.7$. The end-cap and forward regions, spanning $1.5 < |\eta| < 4.9$, are instrumented with LAr calorimetry for both EM and hadronic measurements.

The data sample used in this analysis was taken in 2011 with the LHC operating at a centre-of-mass energy of 7 TeV. Application of beam, detector and data-quality requirements resulted in a total integrated luminosity of 165 pb^{-1}. The trigger required events to contain a leading jet with a transverse momentum (p_{T}), measured at the electromagnetic scale, above 75 GeV and missing transverse momentum above 45 GeV. The detailed trigger specification varied throughout the data-taking period, partly as a consequence of the rapidly increasing LHC luminosity. The trigger reached its full efficiency of > 98 % for events with a reconstructed jet with p_{T} exceeding 130 GeV and more than 130 GeV of missing p_{T}.

3 Object Reconstruction

Jet candidates are reconstructed using the anti-k_t jet clustering algorithm [14, 15] with a distance parameter of 0.4. The inputs to this algorithm are clusters of calorimeter cells [16] seeded by those with energy

[1] ATLAS uses a right-handed coordinate system with its origin at the nominal interaction point in the centre of the detector and the z-axis along the beam pipe. Cylindrical coordinates (r, ϕ) are used in the transverse plane, ϕ being the azimuthal angle around the beam pipe. The pseudorapidity η is defined in terms of the polar angle θ by $\eta = -\ln\tan(\theta/2)$.

significantly above the measured noise. Jet momenta are constructed by performing a four-vector sum over these cell clusters, treating each as an $(E, \vec{p})$ four-vector with zero mass. These jets are corrected for the effects of calorimeter non-compensation and inhomogeneities by using p_{T}- and η-dependent calibration factors based on Monte Carlo (MC) corrections validated with extensive test-beam and collision-data studies [17]. Furthermore, the average additional energy due to pile-up is subtracted using correction constants extracted from an in-situ measurement and the position of the jet is corrected such that the jet direction points to the primary vertex of the interaction instead of the geometrical centre of the ATLAS detector. Only jet candidates with $p_{\mathrm{T}} > 20$ GeV are subsequently retained.

Electron candidates are required to have $p_{\mathrm{T}} > 20$ GeV, to have $|\eta| < 2.47$, and to pass the 'medium' electron shower shape and track selection criteria of Ref. [18]. Muon candidates are required to have $p_{\mathrm{T}} > 10$ GeV and $|\eta| < 2.4$.

Following the steps above, overlaps between candidate jets with $|\eta| < 2.8$ and leptons are resolved using the method of Ref. [19] as follows. First, any such jet candidate lying within a distance $\Delta R < 0.2$ of an electron is discarded, and then any lepton candidate remaining within a distance $\Delta R = 0.4$ of any surviving jet candidate is discarded.

The measurement of the missing transverse momentum two-vector $\vec{P}_{\mathrm{T}}^{\,\mathrm{miss}}$ (and its magnitude $E_{\mathrm{T}}^{\mathrm{miss}}$) is then based on the transverse momenta of all remaining jet and lepton candidates and all calorimeter clusters not associated to such objects. Following this, all jet candidates with $|\eta| > 2.8$ are discarded. Thereafter, the remaining lepton and jet candidates are considered "reconstructed", and the term "candidate" is dropped. The effects of the jet energy scale and resolution on the event reconstruction are discussed in Section 6.

4 Event Selection

Following the object reconstruction described above, events are discarded if any electrons or muons with $p_{\mathrm{T}} > 20$ GeV remain, or if they have any jets failing quality selection criteria designed to suppress detector noise and non-collision backgrounds (see e.g. Ref. [20]), or if they lack a reconstructed primary vertex associated with five or more tracks.

In order to achieve maximal reach over the $(m_{\tilde{g}}, m_{\tilde{q}})$-plane, three signal regions have been defined. When production of squark pairs $\tilde{q}\tilde{q}$ is dominant, only a small number of jets (one per squark from $\tilde{q} \to q\tilde{\chi}_1^0$) is expected. The optimal strategy for the $\tilde{q}\tilde{q}$ region therefore makes requirements on two jets only. When production involves gluinos ($\tilde{g}\tilde{g}$ and $\tilde{q}\tilde{g}$), extra jets are expected from $\tilde{g} \to qq\tilde{\chi}_1^0$. In these regions, requiring at least three jets yields better sensitivity. When $\tilde{g}\tilde{g}$ production dominates, requiring at least four jets yields still better sensitivity. Three signal regions incorporating increasing jet multiplicity requirements are therefore defined (targeting $\tilde{q}\tilde{q}$, $\tilde{g}\tilde{q}$ and $\tilde{g}\tilde{g}$ production, respectively) as shown in Table 1. In this table, $\Delta\phi(\mathrm{jet}, E_{\mathrm{T}}^{\mathrm{miss}})_{\mathrm{min}}$ is the smallest of the azimuthal separations between $\vec{P}_{\mathrm{T}}^{\,\mathrm{miss}}$ and jets with $p_{\mathrm{T}} > 40$ GeV (all jet candidates up to a maximum of three, in descending order of p_{T}). The effective mass, m_{eff}, is defined as the sum of $E_{\mathrm{T}}^{\mathrm{miss}}$ and the magnitudes of the transverse momenta of the two, three or four highest p_{T} jets used to define the signal region.

5 Backgrounds, Simulation and Normalisation

Standard Model (SM) background processes contribute to the event counts in the signal regions. The dominant sources are: W+jets, Z+jets, top pair, multi-jet and single top production. Non-collision backgrounds are negligible. The majority of the W+jets background is composed of $W \to \tau\nu$ events, or $W \to \ell\nu$ events in which no electron or muon candidate is reconstructed. The largest part of the Z+jets background comes from the irreducible component in which $Z \to \nu\bar{\nu}$ generates large $E_{\mathrm{T}}^{\mathrm{miss}}$. Hadronic τ

Signal Region	≥ 2 jets	≥ 3 jets	≥ 4 jets
$E_{\mathrm{T}}^{\mathrm{miss}}$ [GeV]	> 130	> 130	> 130
Leading jet p_{T} [GeV]	> 130	> 130	> 130
Second jet p_{T} [GeV]	> 40	> 40	> 40
Third jet p_{T} [GeV]	–	> 40	> 40
Fourth jet p_{T} [GeV]	–	–	> 40
$\Delta\phi(\mathrm{jet}_i, E_{\mathrm{T}}^{\mathrm{miss}})_{\mathrm{min}}$ $(i = 1, 2, 3)$	> 0.4	> 0.4	> 0.4
$E_{\mathrm{T}}^{\mathrm{miss}}/m_{\mathrm{eff}}$	> 0.3	> 0.25	> 0.25
m_{eff} [GeV]	> 1000	> 1000	> 1000

Table 1: Criteria for admission to each of the three overlapping signal regions. All variables are defined in Section 4. Note that m_{eff} is defined with a variable number of jets, appropriate to each signal region.

decays in $t\bar{t} \rightarrow b\bar{b}\tau\nu qq$ and single top events can generate large $E_{\mathrm{T}}^{\mathrm{miss}}$ and pass the jet and lepton requirements at a non-negligible rate. The multi-jet background in the signal regions is caused by rare instances of poor reconstruction of jet energies in calorimeters leading to 'fake' missing transverse momentum and also by neutrino production in the semileptonic decay of heavy quarks. Extensive validation of MC against data has been performed for each of these background sources and for a wide variety of control regions.

In order to estimate the backgrounds in a consistent fashion, five control regions (CRs) are defined for each of the three signal regions (SRs), giving fifteen CRs in total. The CR event selections are designed to provide data samples enriched in particular background sources. Each ensemble of one SR and five CRs constitutes an independent 'channel' of the analysis. The CR selections are optimised to maintain adequate statistical weight, while minimising as far as possible the systematic uncertainties arising from extrapolation from each CR to the SR.

In each channel the observations in the CRs are used to derive background expectations in the SR through the use of 'Transfer Factors' (TFs) equivalent to the ratios of expected event counts in the CRs and SR. In essence, a TF for each SR and CR pair, derived independently from the CR and SR, provides a conversion factor of 'SR events per CR event'. Multiplication of the conversion factors and the observed numbers of events in the CR yields an estimate of the background in a SR. The TFs for multi-jet processes are estimated using a data-driven technique based upon the smearing of jets in low $E_{\mathrm{T}}^{\mathrm{miss}}$ data events with jet response functions derived from multi-jet dominated data control regions. For the Z+jets, W+jets and top quark processes the TFs are derived from data-validated fully simulated Monte Carlo (MC) event samples. In each channel a likelihood fit is performed to the observed event counts in the SR and five CRs, taking into account correlations in the systematic uncertainties in the TFs. Some uncertainties, such as those arising in MC expectations from jet energy scale calibration and modelling systematics, are reduced in the TFs. The combined fit across all regions ensures that the background estimates are consistent for all processes, taking into account both SM and potential SUSY signal contamination in the CRs.

The irreducible physics background from $Z \rightarrow \nu\bar{\nu}$+jets events is estimated using control regions enriched in a related process with similar kinematics: events with isolated photons and jets (control regions denoted 'CR1'). The reconstructed momentum of the photon is added to the $\vec{P}_{\mathrm{T}}^{\,\mathrm{miss}}$ vector to obtain an estimate of the $E_{\mathrm{T}}^{\mathrm{miss}}$ observed in $Z \rightarrow \nu\bar{\nu}$+jets events. Control regions enriched in $Z \rightarrow ee/\mu\mu$+jets events are used to cross check the photon + jets results and are found to be in good agreement; these results are not, however, used in the final fit.

The background from multi-jet processes is estimated using control regions (control regions CR2)

in which the cut on the minimum jet – $E_{\mathrm{T}}^{\mathrm{miss}}$ ϕ separation is reversed and tightened so as to require $\Delta\phi(\mathrm{jet}, E_{\mathrm{T}}^{\mathrm{miss}})_{\mathrm{min}} < 0.2$. This selects events in which the $E_{\mathrm{T}}^{\mathrm{miss}}$ vector is aligned with one of the three leading jets in the transverse plane. Such a topology is characteristic of events containing mis-measured jets, or neutrino emission from heavy flavour decay within the jet.

The background from $W \to \ell\nu$+jets events is estimated from a sample of events with a lepton (ℓ), significant $E_{\mathrm{T}}^{\mathrm{miss}}$ and a transverse mass of the (ℓ, $E_{\mathrm{T}}^{\mathrm{miss}}$) system between 30 GeV and 100 GeV consistent with the W mass (control regions CR3). In addition, a veto against jets arising from b-quark decays, using a secondary vertex requirement, is applied to remove contamination from events containing top quarks. The lepton in the events is treated as a jet for the computation of the kinematic variables.

The background from top quark events is estimated using the same procedure as that used for $W \to \ell\nu$+jets events, but replacing the b-veto with a b-tag requirement (control regions CR4). This enhances the population of events containing top quark decays relative to that of direct W production events. The resulting TFs include the contribution from events where both top quarks decay leptonically, and also events containing single top production.

MC simulation samples are used to develop the analysis, determine the transfer factors used to estimate W+jets, Z+jets and top quark production backgrounds, and to assess sensitivity to specific SUSY signal models. Samples of simulated multi-jet events from quantum-chromodynamic (QCD) processes are generated with `PYTHIA` [21], using the `MRST2007LO*` modified leading-order parton density functions (PDFs) [22], which are used for all leading-order (LO) MC. Production of top quark pairs is simulated with `MC@NLO` [23, 24] (with a top quark mass of 172.5 GeV) and the Next-to-Leading Order (NLO) PDF set `CTEQ6.6` [25], which is used for all NLO MC. Samples of W and Z/γ^* production with accompanying jets are produced with `ALPGEN` [26]. Single top production is simulated with `MC@NLO` [27, 28]. Fragmentation and hadronization for the `ALPGEN` and `MC@NLO` samples is performed with `HERWIG` [29, 30], using `JIMMY` [31] for the underlying event. SUSY signal samples are generated with `HERWIG++` [32], normalised using NLO cross sections determined by `PROSPINO` [33]. The MC samples are produced using the ATLAS `MC10a` parameter tune [34] and a `GEANT4` [35] based detector simulation [36]. Differing pile-up conditions as a function of the instantaneous luminosity of the LHC machine are taken into account by reweighting events according to the mean number of interactions expected.

6 Systematic Uncertainties

In this analysis systematic uncertainties arise through the use of the transfer factors relating observations in the control regions to background expectations in the signal regions, and from the modelling of the SUSY signal. For the MC-derived transfer factors the primary common sources of systematic uncertainty are the jet energy scale (JES) calibration, jet energy resolution (JER) calibration, MC modelling uncertainties and uncertainty on reconstruction performance in the presence of pile-up.

The JES uncertainty has been measured from the complete 2010 data set using the techniques described in Ref. [17] and, although dependent upon p_{T}, η and proximity to adjacent jets, is around 4%. The JER measured with 2010 data [37] is applied to all MC simulated jets. The difference between the re-calibrated and nominal MC is taken as the systematic uncertainty on the JER. Additional contributions are added to both the JES and the JER uncertainties to take account of the effect of pileup at the relatively high luminosity delivered by the LHC in the 2011 run. Both in-time pileup, multiple collisions within the same bunch-crossing, and out-of-time pileup, which arises from the detector response to neighbouring bunch crossings, will have an effect on the JES and JER. These were studied in detail as a function of the average number of collisions per bunch crossing and by comparing samples taken at 75 and 50 ns bunch spacing. An increase in the JER in the forward region was observed between the 75 and 50 ns data and a systematic uncertainty of $0.07 \times p_{\mathrm{T}}$ is therefore applied to jets with $|\eta| > 2.8$. The combined effects of in-time and out-of-time pileup on the JES are accounted for by an additional conservative systematic

Process	Signal Region		
	≥ 2 jets	≥ 3 jets	≥ 4 jets
$Z \to (\nu\nu)$+jets	5.6 ± 2.1	4.4 ± 1.6	3.0 ± 1.3
$W \to (\ell\nu)$+jets	6.2 ± 1.8	4.5 ± 1.6	2.7 ± 1.3
$t\bar{t}$+ single top	0.2 ± 0.3	1.0 ± 0.9	1.4 ± 0.9
QCD jets	0.05 ± 0.04	0.21 ± 0.07	0.16 ± 0.11
Total	12.1 ± 2.8	10.1 ± 2.3	7.3 ± 1.7
Observed	10	8	7

Table 2: Fitted background components in each signal region compared with observation. The equivalent background estimates obtained using the independent $Z \to ee/\mu\mu$ + jets control region instead of CR1 are in good agreement and serve to validate these results.

which varied from 0 to 7% with $|\eta|$ and p_{T}. Both the JES and JER uncertainties are propagated to the $E_{\mathrm{T}}^{\mathrm{miss}}$. The effect of in-time pileup on other aspects of the standard object selection was also investigated and found to be negligible as would be expected given the high energies of the jets entering the signal samples.

The dominant modelling uncertainty in MC estimates of signal region and control region event counts arises from the treatment of jet radiation as a function of m_{eff}. In order to assess this uncertainty the relevant MC background estimates were recalculated using alternative samples produced with different generators (`ALPGEN` rather than `MC@NLO` for $t\bar{t}$ production) or reduced jet multiplicity (`ALPGEN` processes with 0–4 partons rather than 0–5 partons for W/Z+jets production). Differences in the absolute expectations for SR and CR event counts as high as 100% are observed; the impact on the ratios / transfer factors is, however, much smaller (differences $\lesssim$50%, channel dependent).

Additional uncertainties arising from photon and lepton reconstruction efficiency, energy scale and resolution in CR1, CR3 and CR4, b-tag/veto efficiency (CR3 and CR4) and photon acceptance and cosmic ray backgrounds (CR1) are also considered. Uncertainties in the multi-jet transfer factor estimates are dominated by uncertainties in the modelling of the p_{T} dependence of the Gaussian part of the response function. Other uncertainties including multi-jet seed event statistics and response function statistical and systematic uncertainties are also considered.

Systematic uncertainties on the SUSY signal were estimated through variation of the factorisation and renormalisation scales in `PROSPINO` between half and twice their default values and by considering the PDF uncertainties provided by `CTEQ6`. Uncertainties were calculated for individual production processes (e.g. $\tilde{q}\tilde{q}$, $\tilde{g}\tilde{g}$, etc.).

7 Results, Interpretation and Limits

The observed m_{eff} distributions for each of the channels used in this analysis are shown in Figure 1, together with raw MC background expectations prior to use of the likelihood fitting procedure. The equivalent m_{eff} distributions for the control regions can be found in Appendix A. The number of observed data events and the number of SM events expected to enter each of the signal regions, determined using the likelihood fit, are shown in Table 2. The background model is found to be in good agreement with the data and no excess is observed.

An interpretation of the results is presented in Figure 2 as a 95% confidence exclusion region in the $(m_{\tilde{g}}, m_{\tilde{q}})$-plane for a simplified set of SUSY models with $m_{\tilde{\chi}_1^0} = 0$. In these models the gluino mass and the masses of the squarks of the first two generations are set to the values shown in the figure. All

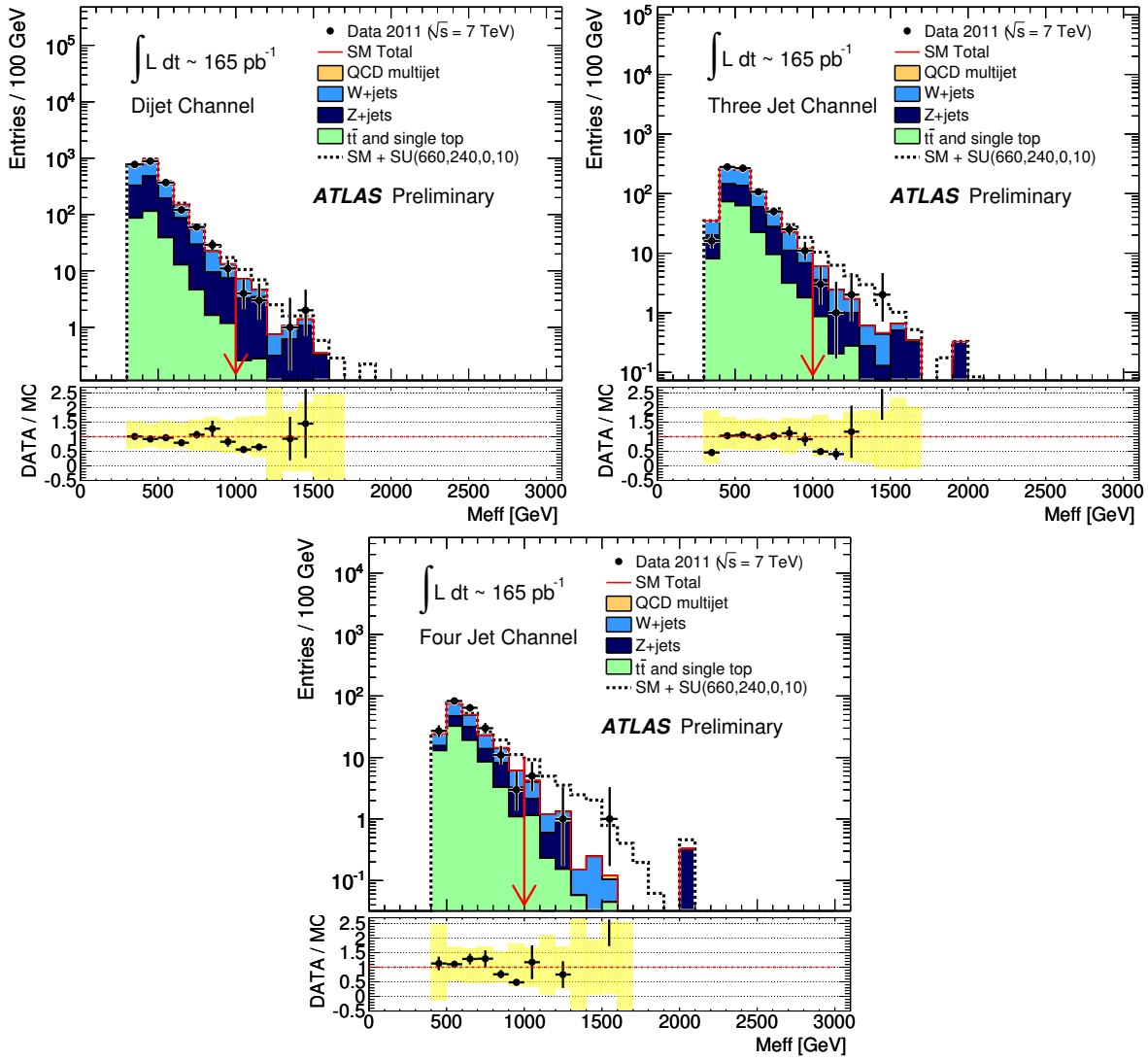

Figure 1: The observed distributions of m_{eff} for the ≥ 2 jet channel (top left), the ≥ 3 jet channel (top right) and the ≥ 4 jet channel (bottom). These plots also show the expected SM contributions after application of all selection criteria obtained from MC simulated samples prior to normalisation using the data-driven likelihood method described in the text. Final cuts on m_{eff} are indicated by the red arrows. For comparison, each plot includes a curve showing the expectation for an MSUGRA/CMSSM reference point with $m_0 = 660$ GeV, $m_{1/2} = 240$ GeV, $A_0 = 0$, $\tan\beta = 10$ and $\mu > 0$. This reference point is also indicated by the star on Figure 3. Below each plot the ratio of the data to the SM expectation is provided. Black vertical bars show the statistical uncertainty from the data, while the yellow band shows the size of the combined Standard Model MC statistical, jet energy scale and jet energy resolution uncertainties.

other supersymmetric particles, including the squarks of the third generation, are decoupled by being given masses of 5 TeV. ISASUSY from ISAJET [38] v7.80 was used to calculate the decay tables, and to guarantee consistent electroweak symmetry breaking. The results are also interpreted in the $\tan\beta = 10$, $A_0 = 0$, $\mu > 0$ slice of MSUGRA/CMSSM[2] [39–44] in Figure 3.

Data from the three channels are used to set the limits, taking the channel with the best expected limit at each point in parameter space. The statistic used to construct the exclusion regions is defined to be the log of the profile likelihood ratio (PLHR) [45, 46] for the observed event count in that region, assuming a non-negative signal contribution (the "power-constrained" method, PCL) [47]. The PLHR for each channel is obtained from the simultaneous fit to the signal region and each of the control regions. The use of transfer factors between all of these regions allows systematic uncertainties and nuisance parameters to be dealt with in a coherent way, preserving any correlations, as described above. The exclusion regions obtained using the CL_s prescription [48] are also shown.

In the limit of light LSPs, with the assumption that the coloured sparticles are directly produced and decay directly to jets and $E_{\mathrm{T}}^{\mathrm{miss}}$, the limit on the gluino mass is approximately 725 GeV, rising to 1025 GeV if the squarks and gluinos are assumed to be mass-degenerate. In the case of a specific SUSY-breaking scenario, i.e. CMSSM/MSUGRA with $\tan\beta = 10$, $A_0 = 0$, $\mu > 0$, the limit on $m_{1/2}$ reaches 455 GeV for low values of m_0, and equal mass squarks and gluinos are excluded below 950 GeV. The adoption of signal selections sensitive to larger jet multiplicities has improved the ATLAS reach at large m_0. The three signal regions considered exclude non-SM cross sections within acceptance of 35, 30 and 35 fb respectively, at 95% confidence.

8 Summary

This note reports a search for new physics in final states containing high-p_{T} jets, missing transverse momentum and no electrons or muons. Good agreement is seen between the numbers of events observed in the three signal regions and the numbers of events expected from SM sources. The three signal regions considered exclude non-SM cross sections within acceptance of 35, 30 and 35 fb respectively, at 95% confidence.

The results are interpreted in both a simplified model containing only squarks of the first two generations, a gluino octet and a massless neutralino, as well as in MSUGRA/CMSSM models with $\tan\beta = 10$, $A_0 = 0$ and $\mu > 0$. In the simplified model, gluino masses below 725 GeV are excluded at the 95% confidence level with the limit increasing to 1025 GeV for equal mass squarks and gluinos. In the MSUGRA/CMSSM models values of $m_{1/2} < 455$ GeV are excluded for low m_0, and equal mass squarks and gluinos are excluded below 950 GeV.

References

[1] L.R. Evans (ed.) and P. Bryant (ed.), *LHC Machine*, J. Instrum. **3** (2008) S08001.

[2] Yu.A. Golfand and E.P. Likhtman, *Extension of the algebra of Poincaré group generators and violation of P invariance*, JETP Lett. **13** (1971) 323-326.
A. Neveu and J.H. Schwartz, *Factorizable dual model of pions*, Nucl. Phys. **B31** (1971) 86-112.
A. Neveu and J.H. Schwartz, *Quark model of dual pions*, Phys. Rev. **D4** (1971) 1109-1111.
P. Ramond, *Dual theory for free fermions*, Phys. Rev. **D3** (1971) 2415-2418.
D.V. Volkov and V.P. Akulov, *Diffractive dissociation of composite particles*, Phys. Lett. **B46**

[2] There are five parameters which are needed to specify a particular MSUGRA/CMSSM model. They are the universal scalar mass, m_0, the universal gaugino mass $m_{1/2}$, the universal trilinear scalar coupling, A_0, the ratio of the vacuum expectation values of the two Higgs fields, $\tan\beta$, and the sign of the higgsino mass parameter, $\mu = \pm$.

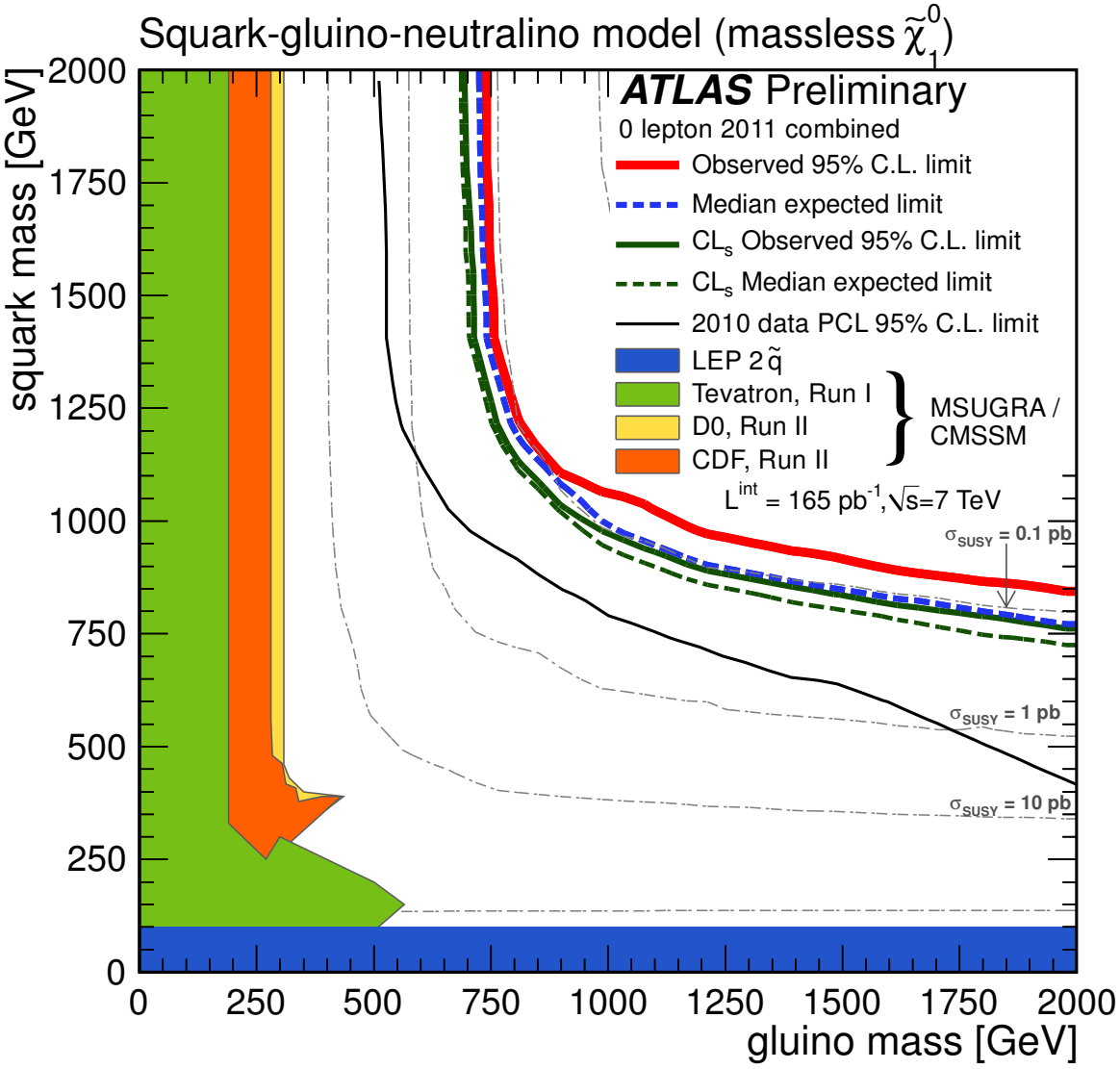

Figure 2: Combined exclusion limits (solid red line) in the ($m_{\tilde{g}}$; $m_{\tilde{q}}$) plane for the simplified squark–gluino model with massless $\tilde{\chi}_1^0$, taking the signal region with the best expected limit per point (limits from individual channels can be found in Appendix B). The dashed-blue line corresponds to the expected 95% C.L. limit and the red line the equivalent observed limit. The dashed green line and the solid green line correspond respectively to the expected and observed limits calculated with the CL$_s$ method. The dot-dashed grey contours show the total supersymmetric cross section. The observed ATLAS limit from 2010 is shown by the solid black line. Note: Tevatron limits [7–10] on $m_{\tilde{q}}$ and $m_{\tilde{g}}$ are marked for searches in the specific context of MSUGRA/CMSSM and are shown purely for illustration, together with limits from LEP [49].

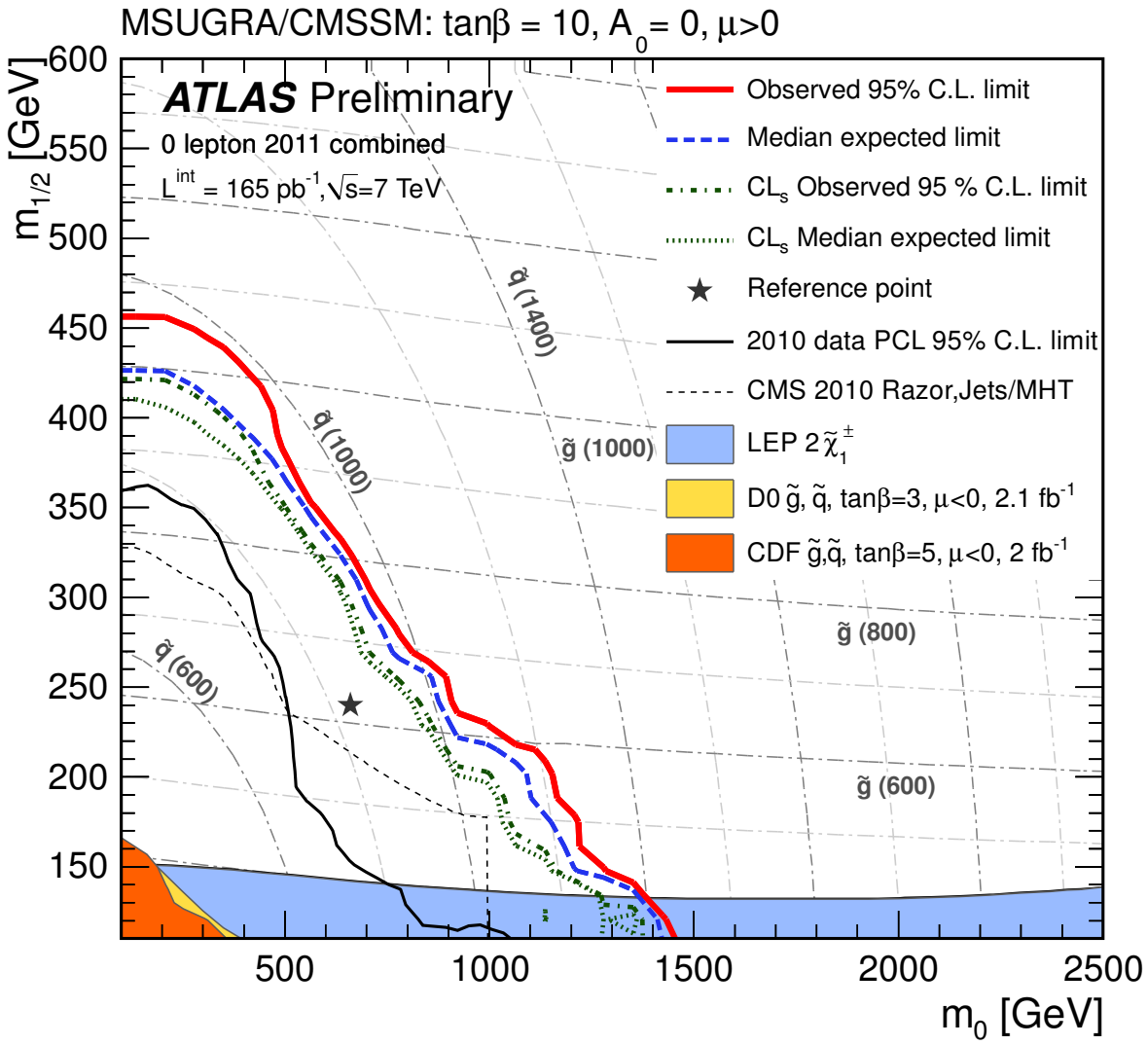

Figure 3: Combined exclusion limits in the (m_0 ; $m_{1/2}$) plane of MSUGRA/CMSSM for which $\tan\beta$ = 10, $A_0 = 0$ and $\mu > 0$ taking the signal region with the best expected limit per point (limits from individual channels can be found in Appendix B). The dashed-blue line corresponds to the expected 95% C.L. limit and the red line the equivalent observed limit. The dotted green line and the dash-dotted green line correspond respectively to the expected and observed limits calculated with the CL_s method. Dot-dashed grey contours of constant gluino and squark mass are displayed at 200 GeV intervals. The observed ATLAS limit from 2010 is shown by the solid black line. The star indicates the position of the MSUGRA/CMSSM reference point with $m_0 = 660$ GeV, $m_{1/2} = 240$ GeV, $A_0 = 0$, $\tan\beta = 10$ and $\mu > 0$ used in Figure 1. Note: ATLAS limits from 2010 are for $\tan\beta = 3$. Tevatron limits are from Refs. [7–10] and are shown purely for illustration. CMS limits are from Ref. [50], and LEP limits from Ref. [51].

(1973) 109-130.
J. Wess and B. Zumino, *Light cone approach to positivity bounds on structure functions for deep inelastic lepton scattering in Weinberg's theory*, Phys. Lett. **B49** (1974) 52-60.
J. Wess and B. Zumino, *Supergauge transformations in four dimensions*, Nucl. Phys. **B70** (1974) 39-50.

[3] P. Fayet, *Spontaneously broken supersymmetric theories of weak, electromagnetic and strong interactions*, Phys. Lett. **B69** (1977) 489.
G. R. Farrar and P. Fayet, *Phenomenology of the production, decay, and detection of new hadronic states associated with supersymmetry*, Phys. Lett. **B76** (1978) 575.

[4] ATLAS Collaboration, *Search for supersymmetry using final states with one lepton, jets, and missing transverse momentum with the ATLAS detector in* $\sqrt{s} = 7$ *TeV pp collisions*, Phys. Rev. Lett. **102** (2011) 131802, arXiv:1102.2357 [hep-ex].

[5] ATLAS Collaboration, *Search for squarks and gluinos using final states with jets and missing transverse momentum with the ATLAS detector in* $\sqrt{(s)} = 7$ *TeV proton-proton collisions*, [arXiv:1102.5290 [hep-ex]].

[6] CMS Collaboration, *Search for Supersymmetry in pp Collisions at 7 TeV in Events with Jets and Missing Transverse Energy*, Phys. Lett. **B698** (2011) 196–218, arXiv:1101.1628 [hep-ex].

[7] D0 Collaboration, *Search for squarks and gluinos in* $p\bar{p}$ *collisions at* $\sqrt{s} = 1.8$ *TeV*, Phys. Rev. Lett. **75** (1995) 618–623.

[8] CDF Collaboration, *Search for gluinos and scalar quarks in* $p\bar{p}$ *collisions at* $\sqrt{s} = 1.8$ *TeV using the missing energy plus multijets signature*, Phys. Rev. Lett. **88** (2002) 041801, arXiv:hep-ex/0106001.

[9] CDF Collaboration, *Inclusive Search for Squark and Gluino Production in* $p\bar{p}$ *Collisions at* $\sqrt{s} =$ *1.96 TeV*, Phys. Rev. Lett. **102** (2009) 121801, arXiv:0811.2512 [hep-ex].

[10] D0 Collaboration, *Search for squarks and gluinos in events with jets and missing transverse energy using 2.1* fb^{-1} *of* $p\bar{p}$ *collision data at* $\sqrt{s} = 1.96$ *TeV*, Phys. Lett. **B660** (2008) 449–457, arXiv:0712.3805 [hep-ex].

[11] CDF Collaboration, *Search for Supersymmetry in* $p\bar{p}$ *Collisions at* $\sqrt{s} = 1.96$*-TeV Using the Trilepton Signature of Chargino-Neutralino Production*, Phys. Rev. Lett. **101** (2008) 251801 arXiv:0808.2446 [hep-ex].

[12] D0 Collaboration, *Search for associated production of charginos and neutralinos in the trilepton final state using 2.3* fb^{-1} *of data*, Phys. Lett. **B680** (2009) 34–43, arXiv:0901.0646 [hep-ex].

[13] ATLAS Collaboration, *The ATLAS Experiment at the CERN Large Hadron Collider*, JINST **3** (2008) S08003.

[14] M. Cacciari, G. P. Salam, and G. Soyez, *The anti-*k_t *jet clustering algorithm*, JHEP **04** (2008) 063, arXiv:0802.1189 [hep-ph].

[15] M. Cacciari and G. P. Salam, *Dispelling the* N^3 *myth for the* k_t *jet-finder*, Phys. Lett. **B641** (2006) 57–61, arXiv:hep-ph/0512210.

[16] ATLAS Collaboration, *Calorimeter Clustering Algorithms : Description and Performance*, ATL-LARG-PUB-2008-002.

[17] ATLAS Collaboration, *Jet energy scale and its systematic uncertainty in proton-proton collisions at $\sqrt{s}$ = 7 TeV in ATLAS 2010 data*, ATLAS-CONF-2011-032.

[18] ATLAS Collaboration, *Expected electron performance in the ATLAS experiment*, ATLAS-PHYS-PUB-2011-006.

[19] ATLAS Collaboration, *Expected Performance of the ATLAS Experiment - Detector, Trigger and Physics*, CERN-OPEN-2008-020. arXiv:0901.0512 [hep-ex].

[20] ATLAS Collaboration, *Data-quality requirements and event cleaning for jets and missing transverse energy reconstruction with the ATLAS detector in proton-proton collisions at a center-of-mass energy of 7 TeV*, ATLAS-CONF-2010-038.

[21] T. Sjostrand, S. Mrenna, and P. Z. Skands, *PYTHIA 6.4 Physics and Manual*, JHEP **0605** (2006) 026, arXiv:hep-ph/0603175.

[22] A. Sherstnev and R. S. Thorne, *Parton Distributions for LO Generators*, Eur. Phys. J. **C55** (2008) 553–575, arXiv:0711.2473 [hep-ph].

[23] S. Frixione and B. R. Webber, *Matching NLO QCD computations and parton shower simulations*, JHEP **06** (2002) 029, arXiv:hep-ph/0204244.

[24] S. Frixione, P. Nason, and B. R. Webber, *Matching NLO QCD and parton showers in heavy flavour production*, JHEP **08** (2003) 007, arXiv:hep-ph/0305252.

[25] P. M. Nadolsky et al., *Implications of CTEQ global analysis for collider observables*, Phys. Rev. **D78** (2008) 013004.

[26] M. L. Mangano, M. Moretti, F. Piccinini, R. Pittau, and A. D. Polosa, *ALPGEN, a generator for hard multiparton processes in hadronic collisions*, JHEP **07** (2003) 001, arXiv:hep-ph/0206293.

[27] S. Frixione, E. Laenen, P. Motylinski, and B. R. Webber, *Single-top production in MC@NLO*, JHEP **03** (2006) 092, arXiv:hep-ph/0512250.

[28] S. Frixione, E. Laenen, P. Motylinski, B. R. Webber, and C. D. White, *Single-top hadroproduction in association with a W boson*, JHEP **07** (2008) 029, arXiv:0805.3067 [hep-ph].

[29] G. Corcella et al., *HERWIG 6.5: an event generator for Hadron Emission Reactions With Interfering Gluons (including supersymmetric processes)*, JHEP **01** (2001) 010, arXiv:hep-ph/0011363.

[30] G. Corcella et al., *HERWIG 6.5 release note*, 2002. arXiv:hep-ph/0210213.

[31] J. M. Butterworth, J. R. Forshaw, and M. H. Seymour, *Multiparton interactions in photoproduction at HERA*, Z. Phys. **C72** (1996) 637–646, arXiv:hep-ph/9601371.

[32] M. Bahr et al., *Herwig++ Physics and Manual*, Eur. Phys. J. **C58** (2008) 639–707, arXiv:0803.0883 [hep-ph].

[33] W. Beenakker, R. Hopker, M. Spira, and P. M. Zerwas, *Squark and gluino production at hadron colliders*, Nucl. Phys. **B492** (1997) 51–103, arXiv:hep-ph/9610490.

[34] ATLAS Collaboration, *First tuning of HERWIG/JIMMY to ATLAS data*, ATL-PHYS-PUB-2010-014.
ATLAS Collaboration *Charged particle multiplicities in pp interactions at* $\sqrt{s} = 0.9$ *and 7 TeV in a diffractive limited phase-space measured with the ATLAS detector at the LHC and new PYTHIA6 tune*, ATLAS-CONF-2010-031.

[35] GEANT4 Collaboration, S. Agostinelli et al., *GEANT4: A simulation toolkit*, Nucl. Instrum. Meth. **A506** (2003) 250–303.

[36] ATLAS Collaboration, *The ATLAS Simulation Infrastructure*, Eur. Phys. J. **C70** (2010) 823–874, arXiv:1005.4568 [physics.ins-det].

[37] ATLAS Collaboration, *Jet energy resolution and selection efficiency relative to track jets from in-situ techniques with the ATLAS Detector Using Proton-Proton Collisions at a Center of Mass Energy* $\sqrt{s} = 7$ *TeV*, ATLAS-CONF-2010-054.

[38] F. E. Paige, S. D. Protopopescu, H. Baer, and X. Tata, *ISAJET 7.69: A Monte Carlo event generator for p p, anti-p p, and e+ e- reactions*, arXiv:hep-ph/0312045.

[39] A. H. Chamseddine, R. L. Arnowitt, and P. Nath, *Locally Supersymmetric Grand Unification*, Phys.Rev.Lett. **49** (1982) 970.

[40] R. Barbieri, S. Ferrara, and C. A. Savoy, *Gauge Models with Spontaneously Broken Local Supersymmetry*, Phys. Lett. **B119** (1982) 343.

[41] L. E. Ibanez, *Locally Supersymmetric SU(5) Grand Unification*, Phys.Lett. **B118** (1982) 73.

[42] L. J. Hall, J. D. Lykken, and S. Weinberg, *Supergravity as the Messenger of Supersymmetry Breaking*, Phys.Rev. **D27** (1983) 2359–2378.

[43] N. Ohta, *Grand unified theories based on local supersymmetry*, Prog.Theor.Phys. **70** (1983) 542.

[44] G. L. Kane, C. F. Kolda, L. Roszkowski, and J. D. Wells, *Study of constrained minimal supersymmetry*, Phys.Rev. **D49** (1994) 6173–6210, arXiv:hep-ph/9312272 [hep-ph].

[45] A. Stuart, K. Ord, and S. Arnold, *Kendall's Advanced Theory of Statistics*, 6th Ed., Oxford Univ. Press (1999) .

[46] G. Cowan, K. Cranmer, E. Gross, and O. Vitells, *Asymptotic formulae for likelihood-based tests of new physics*, Eur. Phys. J. **C71** (2011) 1554, arXiv:1007.1727.

[47] G. Cowan et al., *Power-Constrained Limits*, arXiv:1105.3166 [hep-ex].

[48] A. Read, *Presentation of search results: the CLs technique*, Journal of Physics G: Nucl. Part. Phys. **28** (2002) 2693–2704.

[49] L3 Collaboration *Search for scalar leptons and scalar quarks at LEP.* Phys.Lett. **B580** (2004) 37-49, CERN-EP-2003-059.

[50] CMS Collaboration, *Search for new physics at CMS with jets and missing momentum*, CMS-PAS-SUS-10-005.
CMS Collaboration, *Inclusive search for squarks and gluinos at* $\sqrt{s} = 7$ *TeV*, CMS-PAS-SUS-10-009.

[51] DELPHI Collaboration *Searches for supersymmetric particles in e+ e- collisions up to 208 GeV and interpretation of the results within the MSSM.* Eur.Phys.J. **C31** (2003) 421-479, CERN-EP-2003-007.

A Supplementary m_{eff} plots for control regions used in the analysis

This appendix includes plots of the m_{eff} distributions from each control region separately for the ≥2-, ≥3- and ≥4-jet channels, compared to data. This shows that there is a good understanding of the data in the control regions in all cases, within the statistics available. These distributions, together with the signal region distributions shown in the main body of this note, and the transfer factors, are the primary inputs to the likelihood fits used to determine the exclusion limits.

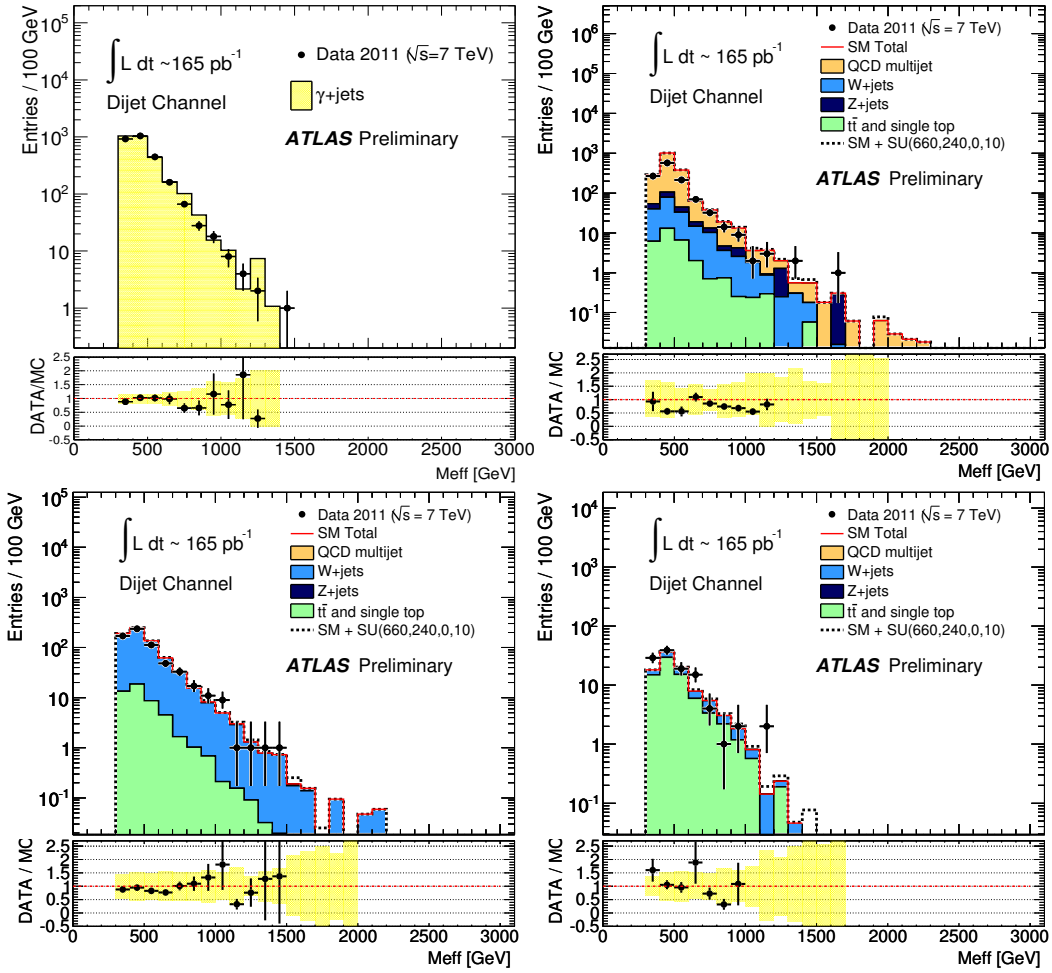

Figure 4: Observed m_{eff} distributions in control regions CR1, CR2, CR3 and CR4 for the inclusive 2-jet channel. These plots also show the expected SM distributions after application of all selection criteria. For CR1 (top left) this is obtained from a MC simulated γ+jet sample prior to normalisation using the data-driven likelihood method described in the text. For CR2, CR3 and CR4 (top right, bottom left and bottom right) the SM contributions are obtained from MC simulated samples prior to normalisation using the data-driven likelihood method described in the text. For comparison, these three plots include a curve showing the expectation for an MSUGRA/CMSSM reference point with $m_0 = 660$ GeV, $m_{1/2} = 240$ GeV, $A_0 = 0$, $\tan\beta = 10$ and $\mu > 0$. In the bottom panel the ratio of the data to the SM expectation is provided. Black vertical bars show the statistical uncertainty from the data, while the yellow band shows the size of the combined Standard Model MC statistical, jet energy scale and jet energy resolution uncertainties.

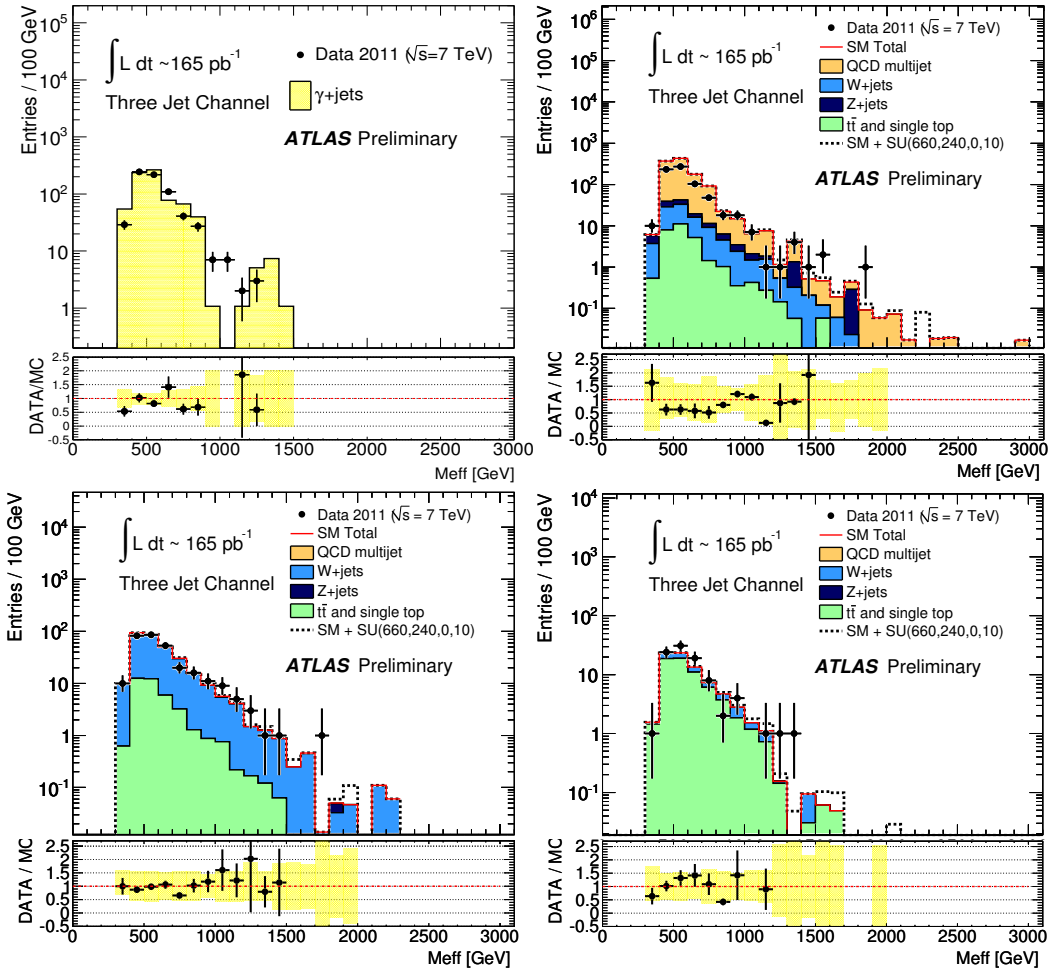

Figure 5: Observed m_{eff} distributions in control regions CR1, CR2, CR3 and CR4 for the inclusive 3-jet channel. These plots also show the expected SM distributions after application of all selection criteria. For CR1 (top left) this is obtained from a MC simulated γ+jet sample prior to normalisation using the data-driven likelihood method described in the text. For CR2, CR3 and CR4 (top right, bottom left and bottom right) the SM contributions are obtained from MC simulated samples prior to normalisation using the data-driven likelihood method described in the text. For comparison, these three plots include a curve showing the expectation for an MSUGRA/CMSSM reference point with $m_0 = 660$ GeV, $m_{1/2} = 240$ GeV, $A_0 = 0$, $\tan\beta = 10$ and $\mu > 0$. In the bottom panel the ratio of the data to the SM expectation is provided. Black vertical bars show the statistical uncertainty from the data, while the yellow band shows the size of the combined Standard Model MC statistical, jet energy scale and jet energy resolution uncertainties.

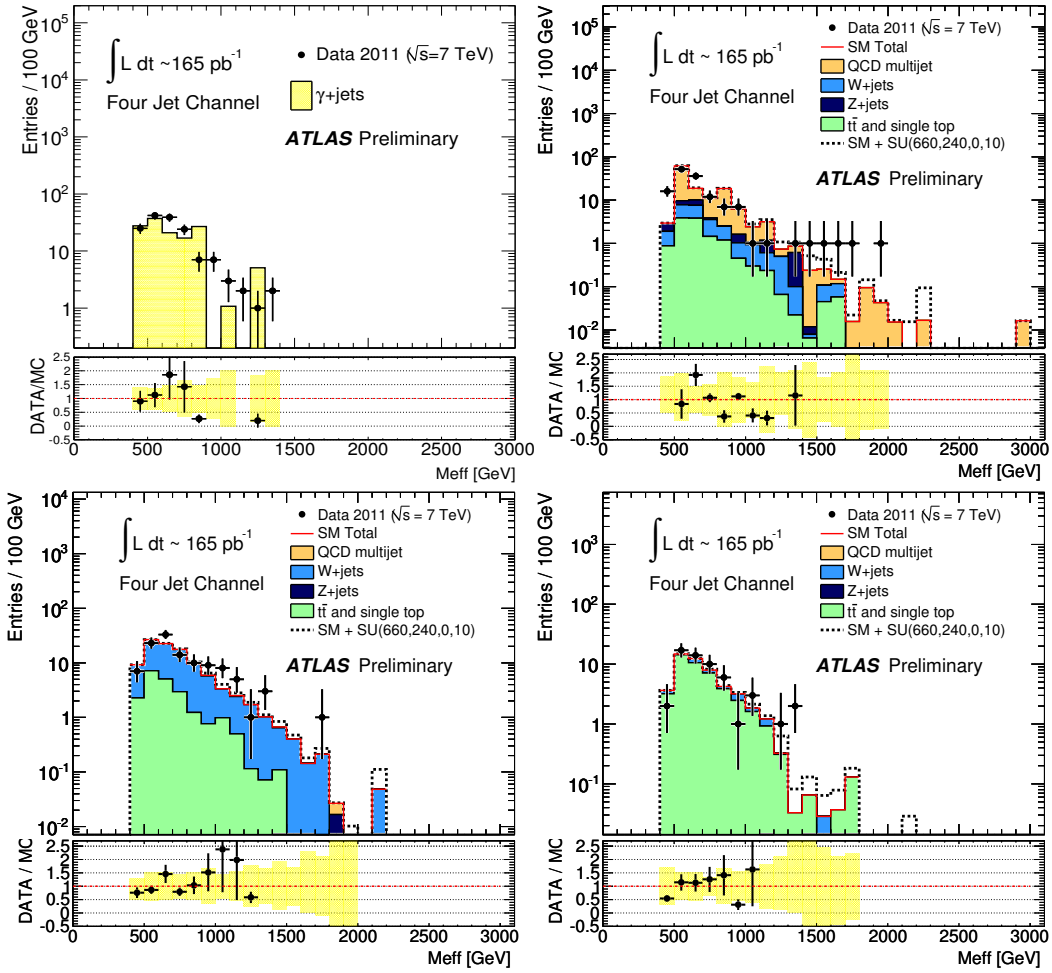

Figure 6: Observed m_{eff} distributions in control regions CR1, CR2, CR3 and CR4 for the inclusive 4-jet channel. These plots also show the expected SM distributions after application of all selection criteria. For CR1 (top left) this is obtained from a MC simulated γ+jet sample prior to normalisation using the data-driven likelihood method described in the text. For CR2, CR3 and CR4 (top right, bottom left and bottom right) the SM contributions are obtained from MC simulated samples prior to normalisation using the data-driven likelihood method described in the text. For comparison, these three plots include a curve showing the expectation for an MSUGRA/CMSSM reference point with $m_0 = 660$ GeV, $m_{1/2} = 240$ GeV, $A_0 = 0$, $\tan\beta = 10$ and $\mu > 0$. In the bottom panel the ratio of the data to the SM expectation is provided. Black vertical bars show the statistical uncertainty from the data, while the yellow band shows the size of the combined Standard Model MC statistical, jet energy scale and jet energy resolution uncertainties.

B Excluded regions in supersymmetry parameter space for each channel separately

These plots show the exclusion limits calculated for each final state channel (≥2-, ≥3- and ≥4-jet) separately. They show the expected limits at 95% confidence and the equivalent limits for $\pm 1\sigma$ variations in the background expectations, as well as the observed 95% confidence limits. The figures in the main body of the note combine these limits by taking the best expected exclusion at each point in parameter space.

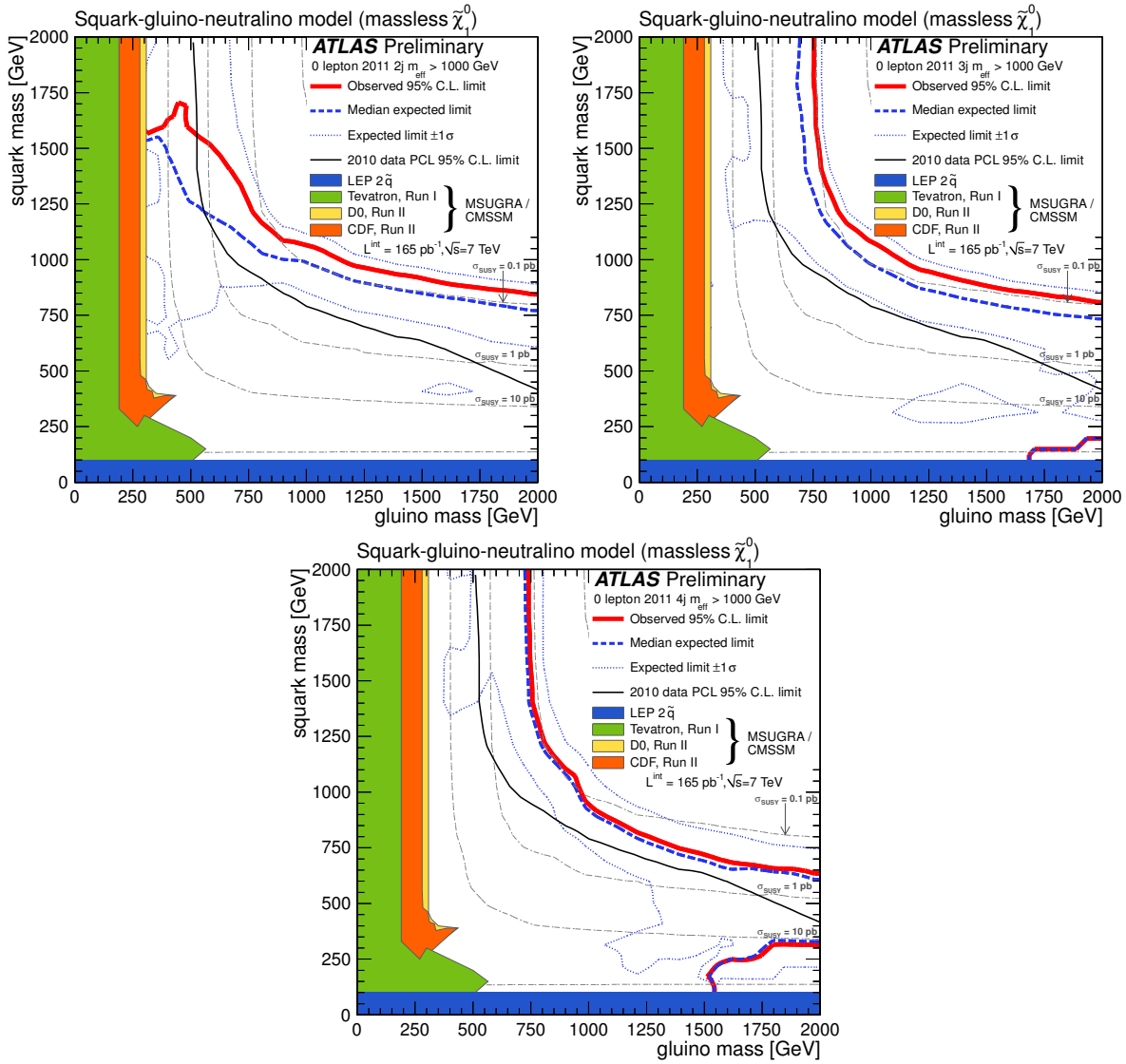

Figure 7: Exclusion limits by channel in the ($m_{\tilde{g}}$, $m_{\tilde{q}}$) plane for the simplified squark–gluino model with massless $\tilde{\chi}_1^0$. The dashed-blue line corresponds to the expected 95% C.L. limit, the dotted blue lines to the limits obtained given a $\pm 1\sigma$ variation in the background expectation. The red line corresponds to the observed limit at 95% confidence. The dot-dashed grey contours show the total supersymmetric cross section. Note: Tevatron limits [7–10] on $m_{\tilde{q}}$ and $m_{\tilde{g}}$ are marked for searches in the specific context of MSUGRA/CMSSM and are shown purely for illustration, together with limits from LEP [49].

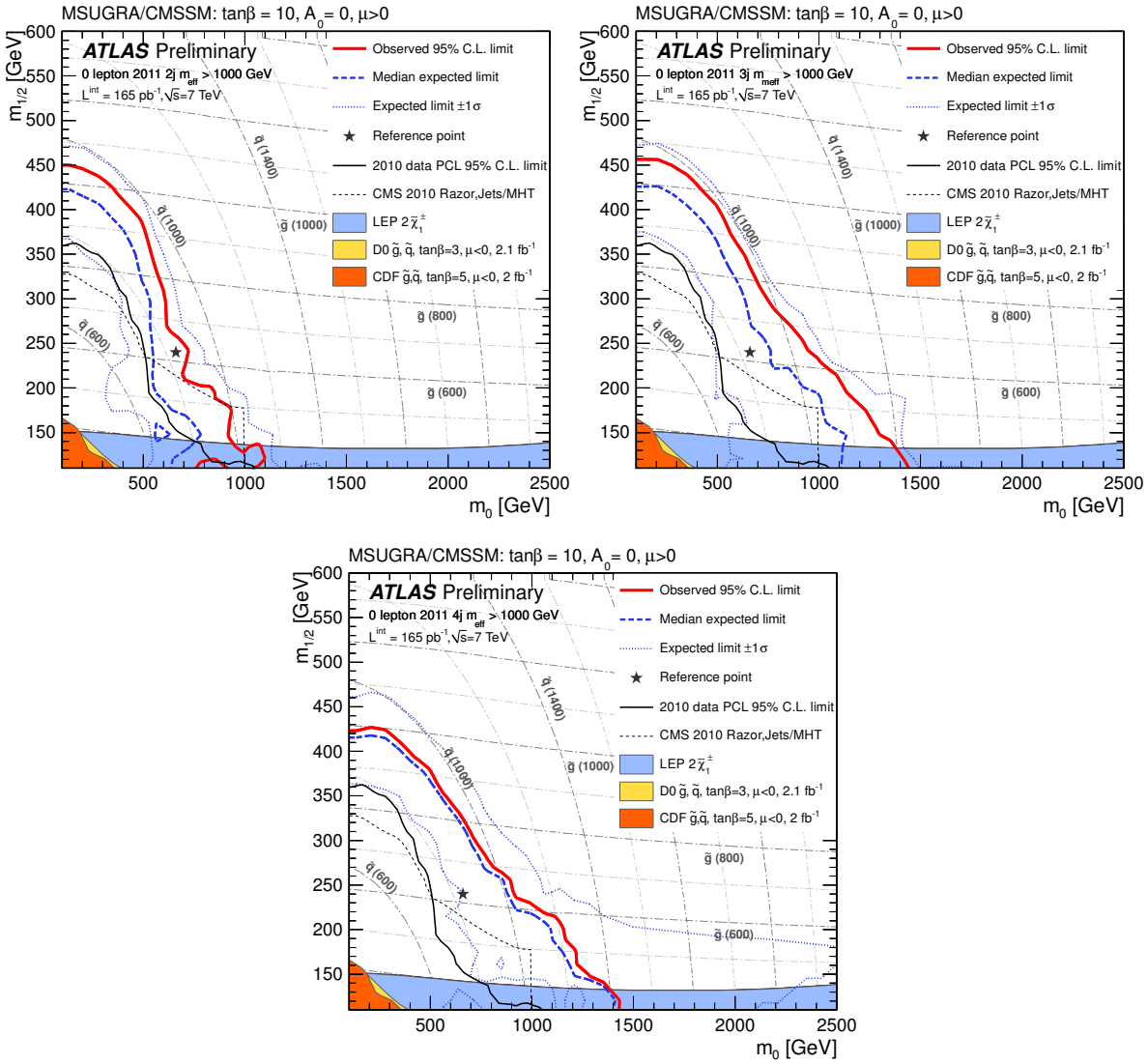

Figure 8: Exclusion limits by channel in the (m_0, $m_{1/2}$) plane of MSUGRA/CMSSM for which $\tan\beta$ = 10, $A_0 = 0$ and $\mu > 0$. The dashed-blue line corresponds to the expected 95% C.L. limit, the dotted blue lines to the limits obtained given a $\pm 1\sigma$ variation in the background expectation. The red line corresponds to the observed limit at 95% confidence. Dot-dashed grey contours of constant gluino and squark mass are displayed at 200 GeV intervals. Note: ATLAS limits from 2010 are for $\tan\beta = 3$. Tevatron limits are from Refs. [7–10] and are shown purely for illustration. CMS limits are from Ref. [50], and LEP limits from Ref. [51].

C Event display of the highest m_{eff} event recorded in this data sample.

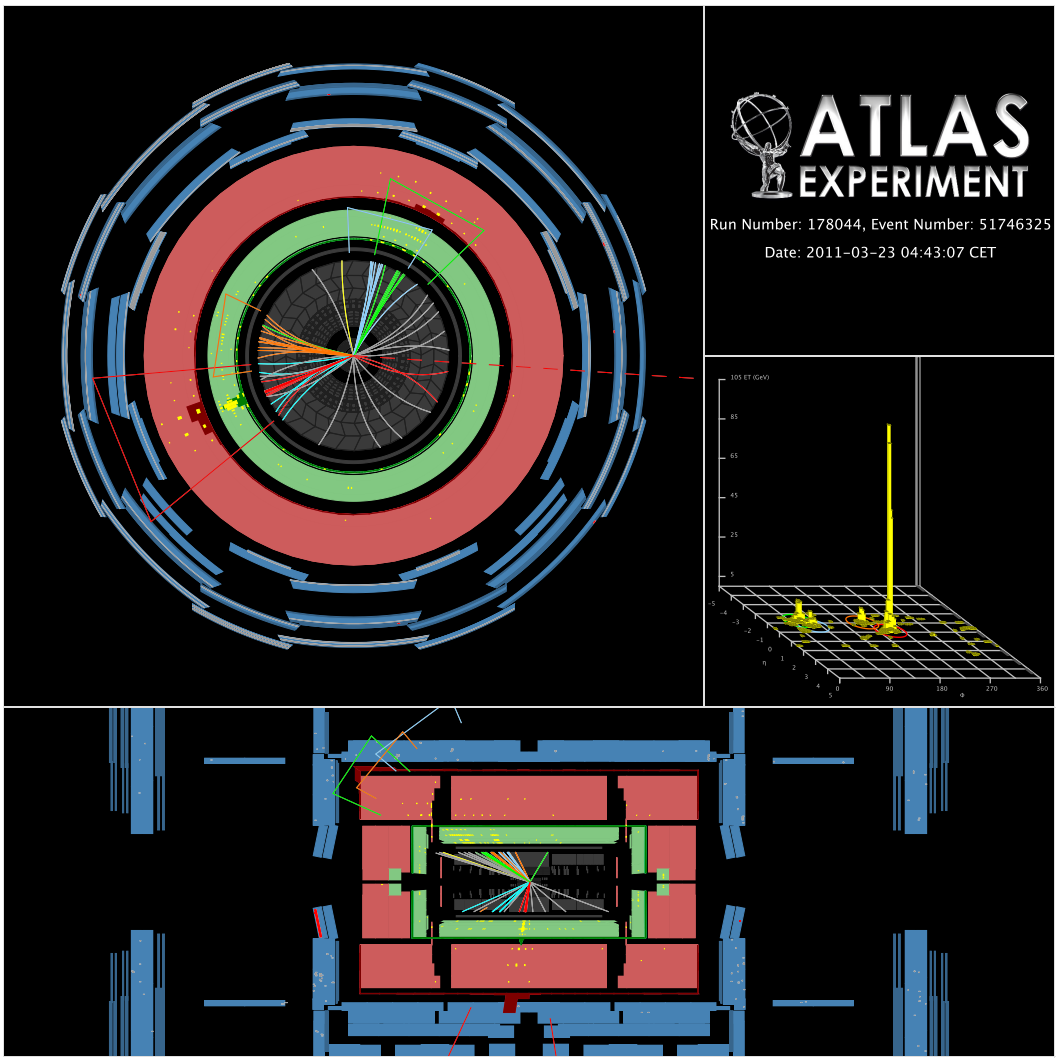

Figure 9: A display of the reconstructed event with the highest m_{eff} found in the data sample used for this note. This event possesses four jets with $p_{\text{T}} > 40$ GeV ($p_{\text{T}} = 636$, 189, 96 and 81 GeV respectively), $E_{\text{T}}^{\text{miss}} = 547$ GeV and $m_{\text{eff}} = 1548$ GeV (calculated using the leading four jets).